Microstructural analysis of rapidly solidified aluminium-nickel alloys

Ilbagi, A.; Delshad Khatibi, P.; Swainson, I. P.; Reinhart, G.; Henein, H.

Publisher's version / Version de l'éditeur:
https://doi.org/10.1179/1879139511Y.0000000006
Canadian Metallurgical Quarterly, 50, 3, pp. 295-302, 2011-07-01

Microstructural analysis of rapidly solidified aluminium–nickel alloys

A. Ilbagi*[1], P. Delshad Khatibi[1], I. P. Swainson[2], G. Reinhart[3,4] and H. Henein[1]

Powders of Al–50 wt-%Ni and Al–36 wt-%Ni were produced using the impulse atomisation technique, a rapid solidification technique. The molten droplets were cooled in flight by the stagnant helium or nitrogen in the atomising chamber. The resulting powders were sieved into different size ranges. X-ray diffraction and neutron diffraction were used in order to quantify the phase fractions in the samples. Profile refinement, using the computer software GSAS, was used to calculate the weight fraction of the existing phases, namely Al_3Ni_2, Al_3Ni and Al, as a result of different processing parameters. The Scheil–Gulliver model was applied to investigate the extent to which it can predict phase fractions in the Al–Ni system. In Al–50 wt-%Ni, by increasing cooling rate, the ratio of Al_3Ni to Al_3Ni_2 approaches that of Scheil–Gulliver's prediction. Opposite behaviour was observed in Al–36 wt-%Ni. In addition, from the profile refinement, the effect of composition and cooling rate on the lattice parameter of Al_3Ni_2 was investigated. In Al–36 wt-%Ni, the *c/a* ratio is significantly smaller than the stoichiometric *c/a* ratio of Al_3Ni_2, and it decreases with increasing cooling rate. On the other hand, for Al–50 wt-%Ni, the *c/a* ratio is much closer to the stoichiometric value and it increases with increasing cooling rate.

On a produit des poudres d'Al-50% en poids de Ni et d'Al-36% en poids de Ni en utilisant la technique d'atomisation par impulsion, une technique de solidification rapide. Les gouttelettes fondues étaient refroidies en vol par l'hélium ou l'azote stagnants dans la chambre d'atomisation. Les poudres résultantes étaient tamisées en différentes gammes de taille. On a utilisé la diffraction des rayons X et la diffraction des neutrons pour quantifier les fractions de phase dans les échantillons. Le raffinement du profil, obtenu grâce au logiciel d'ordinateur GSAS, était utilisé pour calculer la fraction de poids des phases existantes, soit Al_3Ni_2, Al_3Ni et Al, comme résultat des différents paramètres de traitement. On a appliqué le modèle de Scheil-Gulliver pour vérifier à quel point il peut prédire les fractions de phase du système Al-Ni. Pour l'Al-50% en poids de Ni, en augmentant la vitesse de refroidissement, le rapport d'Al_3Ni à Al_3Ni_2 s'approche de celui de la prédiction de Scheil-Gulliver. On a observé le comportement opposé pour l'Al-36% en poids de Ni. De plus, à partir du raffinement du profil, on a étudié l'effet de la composition et de la vitesse de refroidissement sur le paramètre de réseau de l'Al_3Ni_2. Pour l'Al-36% en poids de Ni, le rapport c/a est significativement plus petit que le rapport c/a stoechiométrique de l'Al_3Ni_2, et il diminue avec une augmentation de la vitesse de refroidissement. D'un autre côté, pour l'Al-50% en poids de Ni, le rapport c/a est beaucoup plus près de la valeur stoechiométrique et il augmente avec une augmentation de la vitesse de refroidissement.

Keywords: Rapid solidification, Scheil–Gulliver, Neutron diffraction, Rietveld refinement, Al_3Ni_2

[1]Department of Chemical and Materials Engineering, CME 213, University of Alberta, Edmonton, Alberta T6G 2G6, Canada
[2]Canadian Neutron Beam Centre, National Research Council of Canada, Chalk River Laboratories, Station 18, Chalk River, Ont. K0J 1J0, Canada
[3]Aix-Marseille Université, IM2NP, Campus Saint-Jérôme, Case 142, 13397 Marseille Cedex 20, France
[4]CNRS, IM2NP (UMR 6242), Campus Saint-Jérôme, Case 142, 13397 Marseille Cedex 20, France

*Corresponding author, email ilbagi@ualberta.ca

This paper is part of a special issue on Aerospace Materials Development, Manufacturing and Application

Introduction

Recently, peritectic reactions have attracted the attention of many scientists who try to understand and simulate this important transformation that occurs in many metallic systems.[1,2] This is mostly because many of the

Published by Maney on behalf of the Institute
Received 10 February 2011; accepted 19 April 2011
DOI 10.1179/1879139511Y.0000000006

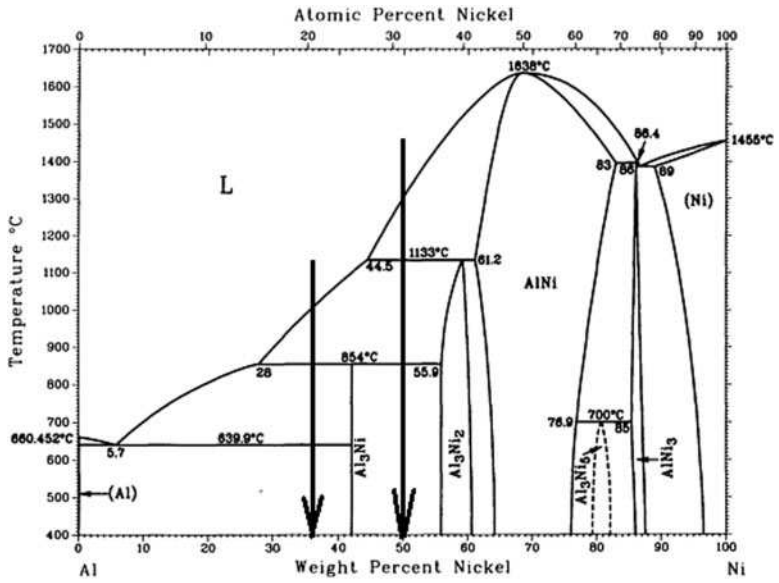

1 Al–Ni phase diagram[3]: arrows show compositions investigated in this research

intermetallic phases that show high strength, high ductility and high corrosion resistance at elevated temperatures are produced by peritectic reactions. These material characteristics are greatly influenced by microstructure evolution during the peritectic reaction, which itself is affected by processing parameters during production. In this work, the aluminium rich side of the Al–Ni phase diagram (*see* Fig. 1)[3] has been chosen as a model system for the investigation of the effects of cooling rate on the microstructure and the phase fractions during the solidification of Al–36 wt-%Ni and Al–50 wt-%Ni.

Solidification path

Equilibrium

Comparison between the solidification of Al–36 wt-%Ni and Al–50 wt-%Ni alloys is interesting as the former experiences only one peritectic reaction at 854°C, while the latter goes through two peritectic reactions at 1133 and 854°C. From the phase diagram, the solidification of an Al–50 wt-%Ni alloy can be explained as follows (*see* Fig. 1).

At 1133°C, the primary AlNi dendrites, which had started to solidify at ~1300°C, react with the surrounding liquid in a peritectic reaction to form Al_3Ni_2. It is expected that at this composition, the entire primary AlNi phase transforms to Al_3Ni_2. The peritectic product grows until it reaches the second peritectic reaction at 854°C, where it reacts with the remaining liquid to form Al_3Ni. At this composition, this reaction is not expected to go to completion, and a final composition consisting of 58 wt-%Al_3Ni_2 and 42 wt-%Al_3Ni should form. The equilibrium phase diagram predicts no eutectic aluminium for this composition.

The story for the Al–36 wt-%Ni is different as at this composition, the equilibrium phase diagram shows that the Al_3Ni_2 forms as the primary phase. It then goes through the peritectic reaction at 854°C, where it is believed to transform entirely to Al_3Ni. The remaining liquid solidifies in a eutectic reaction into aluminium and Al_3Ni. The resulting composition at the end of equilibrium solidification, as predicted by the phase diagram, must contain almost 85 wt-%Al_3Ni and 15 wt-% aluminium and no primary Al_3Ni_2.

St John and Hogan[4] in 1987 showed that the composition gradient within the peritectic phase would strongly influence the rate of peritectic transformation. Based on their analysis, a peritectic reaction is extremely slow when the product is of fixed composition or has very narrow homogeneity range. This is the case for Al_3Ni. This intermetallic has a fixed composition at 42 wt-%Ni, rendering its formation from the peritectic reaction at 854°C very sluggish. In such cases, the undercooling and/or high cooling rates can result in metastable conditions. This metastability may occur in the form of a new phase, different proportions of phases or higher solute content.

Scheil–Gulliver equation

The Scheil–Gulliver equation is used to describe solute redistribution during solidification of an alloy. This model assumes perfect mixing in liquid and no diffusion in solid to predict solute distribution during solidification. However, for example, in the case of Al–36 wt-% Ni, the initial reaction of the liquid with the properitectic phase, Al_3Ni_2, would leave an envelope of the peritectic product, Al_3Ni, around the primary phase, Al_3Ni_2. Further transformation requires the diffusion of Ni through Al_3Ni envelope. This does not follow the Scheil–Gulliver assumption. Hence, the peritectic reaction does not proceed in the simulation of solidification using a Scheil–Gulliver model.[5] Therefore, the fraction of the peritectic product, Al_3Ni, predicted by the Scheil–Gulliver equation, will be an underestimation of the Al_3Ni phase fraction produced during equilibrium cooling. However, in some cases, this might be a good estimate. In this paper, the extent to which the Scheil–Gulliver equation can predict the phase fractions in Al–36 wt-%Ni and Al–50 wt-%Ni will be investigated by comparing the phase fractions measured using neutron

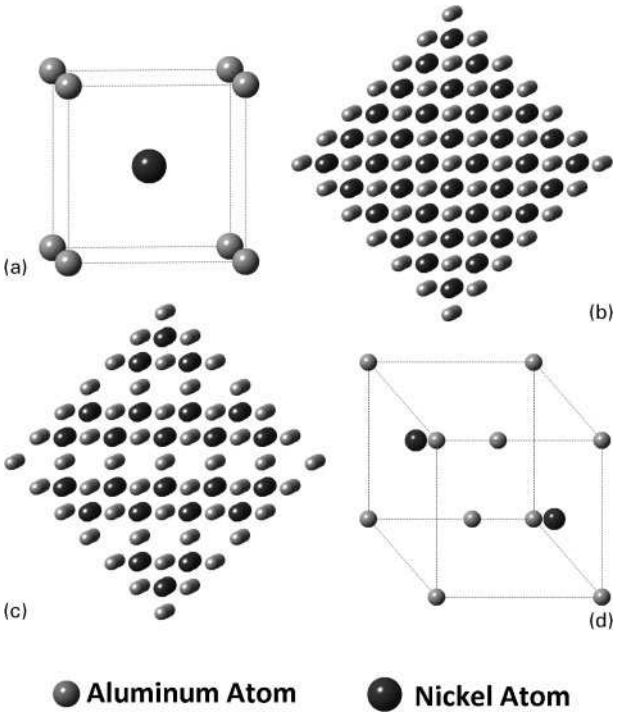

2 *a* unit cell of AlNi, *b* several unit cells of AlNi, *c* formation of Al_3Ni_2 from AlNi by removing every third sheet of nickel atoms perpendicular to one of threefold axes of cube and *d* unit cell of Al_3Ni_2: difference in size of aluminium and nickel atoms was dictated by drawing software and has no scientific meaning

diffraction (ND) and X-ray diffraction (XRD) with those calculated by Scheil–Gulliver equation.

Previously, Ilbagi *et al.*[6] showed that in Al–50 wt-%Ni, increasing the cooling rate, either by using helium instead of nitrogen as cooling gas, or by decreasing particle size from 925 to 256 μm, decreased the weight fraction of Al_3Ni and Al while it increased the weight fraction of Al_3Ni_2. Although it was stated that Scheil–Gulliver model cannot simulate the peritectic reactions accurately, it will be shown that in the case of Al–50 wt-%Ni, at higher cooling rates, the phase fractions approach that of Scheil–Gulliver simulation.

To calculate the phase fractions using Scheil–Gulliver model, in the case of Al–50 wt-%Ni, at 1133°C, the fractions of solid (AlNi) and liquid can be calculated using the compositions shown on the phase diagram (C_S=57·97 at-%Al, C_L=73·07 at-%Al and C_0=68·50 at-% Al). For the next reaction, at 854°C, C_0 has the composition of the remaining liquid from the previous step, which was 73·07 at-%Al. At this temperature, C_L=84·83 at-%Al and C_S=63·18 at-%Al. Using Scheil–Gulliver equation, the amount of Al_3Ni_2 that has formed is calculated. Since it was previously showed[6] that all AlNi transforms to Al_3Ni_2, the total amount of Al_3Ni_2 is calculated by adding the results of the first two steps together. Step 3, at 639·9°C, gives the fraction of proeutectic Al_3Ni and it is similar to step two. In this case, the last liquid composition from step 2, 84·83 at-%Al, is used as the initial composition for step 3. C_S is 75·03 at-%Al and C_L is 97·30 at-%Al. The remaining liquid of this step transforms to Al and Al_3Ni in a eutectic transformation. From these calculations, the ratio of Al_3Ni to Al_3Ni_2 for Al–50 wt-%Ni is 0·33. The same procedure can be applied to Al–36 wt-%Ni and the ratio of Al_3Ni to Al_3Ni_2 is 1·74.

Al_3Ni_2 lattice parameter

In this paper, the effect of cooling rate and composition on the lattice parameter of Al_3Ni_2 is also investigated.

It is known that the Al_3Ni_2 structure is similar to that of AlNi structure with 33% of the nickel sites vacant at the stoichiometric composition. The vacancies are ordered in a way that every third sheet of nickel atoms perpendicular to one of the threefold axes of the cube is absent. The unit cell of AlNi and the process of its transformation to Al_3Ni_2 are shown in Fig. 2 [Images were generated using CrystalMaker, a crystal and molecular structures program for Mac and Windows. CrystalMaker Software Ltd, Oxford, UK (www.crystalmaker.com)]. This ordering transforms the crystal structure from cubic to rhombohedral by unequal changes of the parameters c and a.[7] The cube diagonal in AlNi becomes the c axis in Al_3Ni_2 ($c=a'3^{1/2}$, where a' is the cube edge) and the cube face diagonal becomes a axis of Al_3Ni_2 unit cell ($a=a'2^{1/2}$). Therefore, it is expected that the axial ratio to be c/a=1·225. However, due to the collapse along the c axis, as a result of the missing planes, it drops to 1·2132 at stoichiometric Al_3Ni_2.[8] Taylor and Doyle[8] also showed that the c/a ratio falls continuously across the phase with increasing aluminium content of Al_3Ni_2. On the other hand, Bao *et al.*[9] showed that the stoichiometric amounts of aluminium and nickel in Al_3Ni_2 are sensitive to the cooling rate. They applied Rietveld refinement to ND and XRD patterns from gas atomised powders to show that by decreasing the particle size from 500 to 25 μm, which corresponds to the increasing cooling rate, the ratio of Al/Ni decreases. However, the effect of cooling rate on the lattice parameter of Al_3Ni_2 has not yet been established very well.

In this work, the lattice parameter ratio of Al_3Ni_2 will be measured using the Rietveld refinement on ND patterns and the effect of cooling rate on c/a ratio at two different compositions, Al–36 wt-%Ni and Al–50 wt-% Ni, will be discussed.

Table 1 Alloy compositions and atomisation conditions

Atomisation run no.	Atomisation atmosphere	Nominal composition	No. of orifices	Actual composition
080804	He	Al–36 wt-%Ni	37	Al–36·1 wt-%Ni
100824	N_2	Al–36 wt-%Ni	37	Al–36·1 wt-%Ni
080731	He	Al–50 wt-%Ni	37	Al–49·8 wt-%Ni
080916	N_2	Al–50 wt-%Ni	37	Al–49·6 wt-%Ni

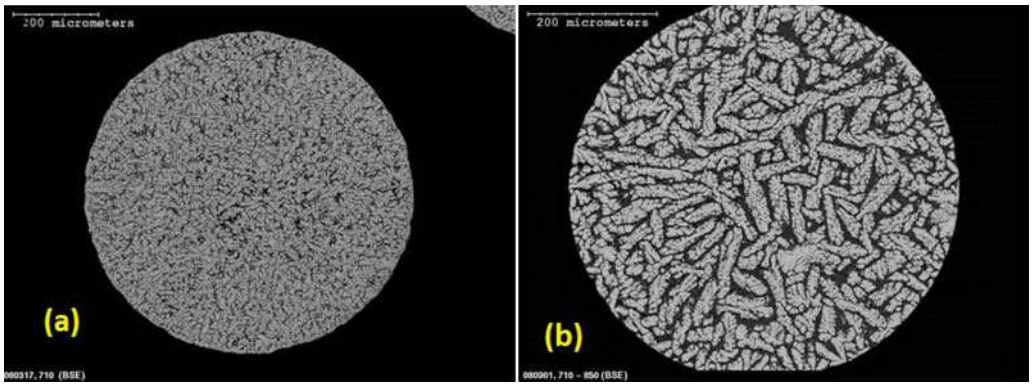

3 Two particles of Al–50 wt-%Ni atomised in *a* helium and *b* nitrogen: particle size is 780 μm

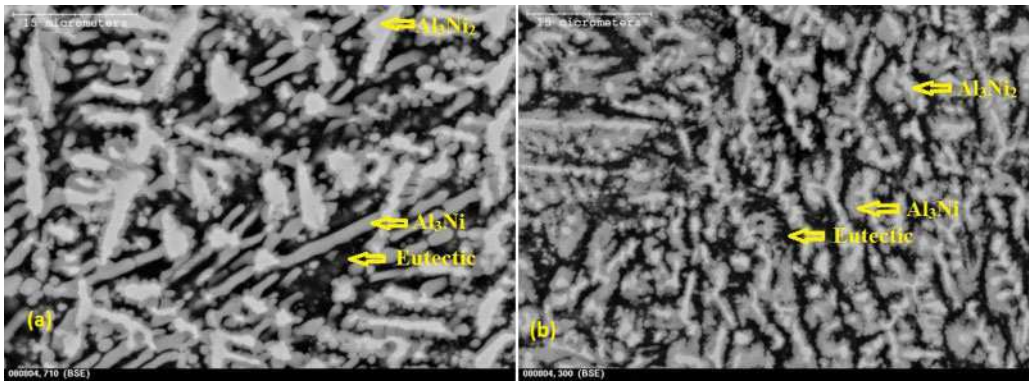

4 Two particles of Al–36 wt-%Ni atomised in helium with particle size of *a* 780 μm and *b* 328 μm

Experimental

Two different compositions of Al–Ni alloys (36 and 50 wt-%Ni) were impulse atomised under different gas atmospheres (*see* Table 1 for details). This technique differs from the conventional gas atomisation technique as it is a single fluid atomisation process. A liquid jet is generated when the molten metal is pushed through small orifices placed at the bottom of a crucible. It then breaks up into spherical droplets by Rayleigh instability. The falling droplets lose heat to the surrounding stagnant gas and solidify before reaching the bottom of the atomisation vessel. The details of this technique can be found elsewhere.[10] Each alloy was produced by melting 99·9% pure Al and Ni (Alfa Aesar). The melt was atomised after holding it for 30 min at 100°C above its liquidus temperature. The solidified particles were washed and sieved into different size ranges, from 100 to 1000 μm, according to Metal Powder Industries Federation Standard 05.[11] The chemical composition of each sample was measured using inductively coupled plasma atomic emission spectroscopy and is shown in Table 1. Neutron diffraction, XRD and scanning electron microscopy (SEM) were then used to characterise the powders.

Scanning electron microscopy was performed using an S-2700-C Hitachi SEM with 20 keV electron beam energy. At least 30 measurements were conducted to measure secondary dendrite arms spacing (SDAS) for each particle size.

The ND experiments were conducted at Oak Ridge National Laboratory and Atomic Energy of Canada Limited, Chalk River, facilities using a neutron beam of 1·33 Å wavelength. The XRD experiments on a particle size range from 181 to 1200 μm were carried out using K_α radiation from Cu source on a Rigaku Denki Rotaflex RU-200B X-ray generator at University of Alberta. While the depth of penetration of neutrons is almost three orders of magnitude higher than that of XRD, which is only a few micrometres, XRD was used in addition to ND to get an idea of the difference between phase fractions on the surface and within the bulk of the particles. The ND results give the mean value of the weight percentage Al_3Ni_2, Al_3Ni and Al in 3–5 g powder sample. The values obtained for the same phases from XRD only come from the surface of the particles. In order to obtain phase fractions from the diffraction methods, Rietveld analysis was performed using the software General Structure Analysis System (GSAS).[12,13] Lattice parameters of Al_3Ni_2 were also measured as a part of diffraction pattern refining process.

Results and discussion

Scanning electron microscopy

Figure 3 shows the SEM microstructure of two impulse atomised particles of Al–50 wt-%Ni. The particle in Fig. 3*a* was atomised in helium while the particle in Fig. 3*b* was atomised in nitrogen. Visual observation of these particles shows that both particles have dendritic

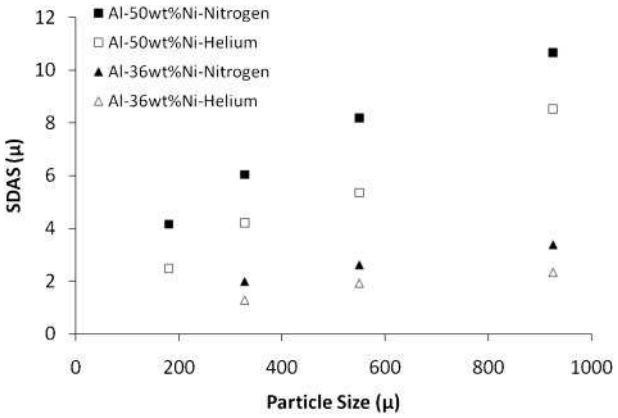

5 Effect of particle size, gas type and composition on SDAS

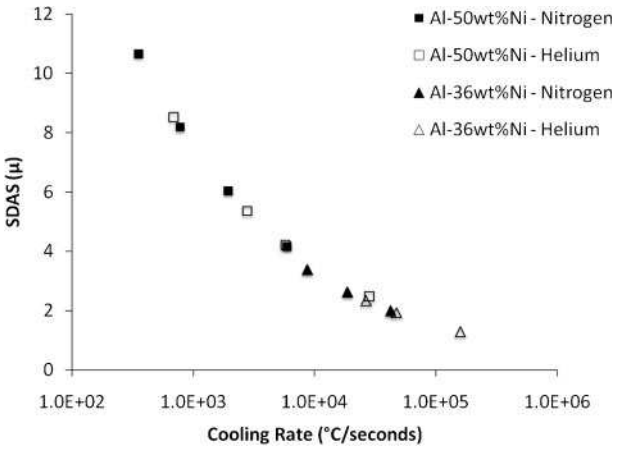

6 Calculated cooling rate of Al–50 wt-%Ni and Al–36 wt-% Ni, atomised both in helium and nitrogen

microstructure with almost uniform distribution along the cross-section. Since the thermal conductivity of helium is significantly higher than that of nitrogen,[14] the particle in Fig. 3*a* has lost heat faster than the one in Fig. 3*b*, and therefore formed a more refined microstructure.

Figure 4 shows two Al–36 wt-%Ni particles of different sizes, atomised in helium. Three different greyscales representing three different phases can be seen in these images. Energy dispersive X-ray (EDX) analysis of the white phase observed in the core of dendrites showed that it contains 39 at-% nickel, which is close to that of Al_3Ni_2. These dendrites are surrounded by a light grey phase. From EDX, it was found that this phase contains 24 at-% nickel. The morphology and the composition of this phase suggest that it is the peritectic product, Al_3Ni. The dark grey structure, which contains >95 at-% aluminium, is the eutectic that formed during the last stage of the solidification.

The comparison of the scales of these microstructures shows that the smaller the particle, the finer the microstructure.

Figure 5 shows the SDAS of different particle sizes of both Al–36 wt-%Ni and Al–50 wt-%Ni atomised in helium and nitrogen. From this figure, it can be observed that particles with higher amount of nickel

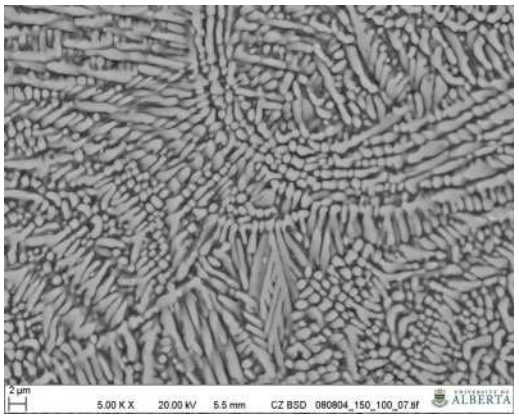

7 Al–36 wt-%Ni particle with diameter of 150 μm cooled in helium

are coarser than the particles with lower nickel. In addition, it is evident that decreasing particle size, as well as using helium rather than nitrogen, resulted in finer microstructure.

Kurz and Fisher[15] showed that the SDAS λ is proportional to the cube of solidification time t as it is a function of the extent of coarsening that occurs during solidification (*see* equations (1) and (2))

$$\lambda = 5{\cdot}5(Mt)^{1/3} \tag{1}$$

with

$$M = \frac{D\Gamma \ln\left(C_1^{\mathrm{m}}/C_0\right)}{m(1-k)\left(C_0 - C_1^{\mathrm{m}}\right)} \tag{2}$$

where Γ is the Gibbs–Thomson coefficient, D is the diffusion coefficient of solute in the liquid, m is the slope of the liquidus line, k is distribution coefficient, C_1^{m} is the composition of the last liquid to solidify and C_0 is the overall composition. Except for Γ and D, the rest of the parameters in equation (2) can be found from the phase diagram, where it was assumed that the liquidus line is linear. The role of diffusion coefficient in the coarsening of dendrites is crucial; however, experimental data for diffusion of Al in Al–Ni alloys are lacking. Therefore, the values suggested by Tourret and Gandin[1] were used, where $\Gamma = 1 \times 10^{-8}$ m K and $D = 1 \times 10^{-8}$ $m^2\ s^{-1}$.

Using the calculated values of M, the measured SDAS and equation (1), the solidification time of the primary phase can be calculated. It is assumed that the dendrite arm coarsening has generally occurred before the first peritectic reaction takes place. Dividing the solidification range of the primary phase by the calculated solidification time gives the primary phase cooling rate. The measured SDAS as a result of different cooling rates was plotted in Fig. 6. It is shown that particles of Al–36 wt-%Ni achieved higher cooling rates than those of Al–50 wt-% Ni. In addition, at each composition, those atomised in helium have experienced higher cooling rates. From Fig. 6, the SDAS can be related to the cooling rate using equations (3) and (4) for Al–50 wt-%Ni and Al–36 wt-% Ni respectively

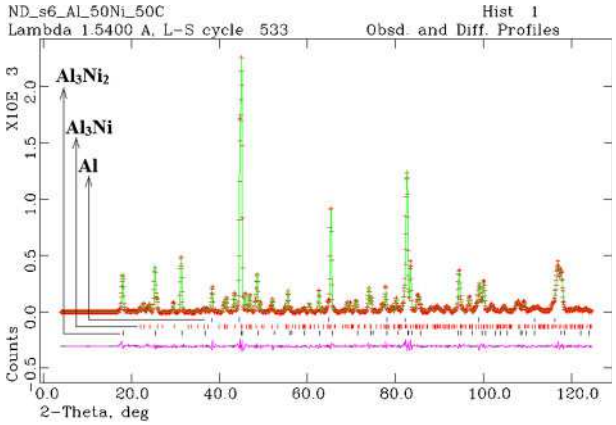

8 Neutron diffraction profile refinement using software GSAS of Al–50 wt-%Ni, with diameter of 328 μm, atomised in helium: experimental points are shown in symbols (+) and calculated diffraction pattern is shown as curve; difference between measured and calculated results is shown as curve at bottom of figure; vertical bars show diffraction peak position for Al (top), Al_3Ni (middle) and Al_3Ni_2 (bottom) phases respectively

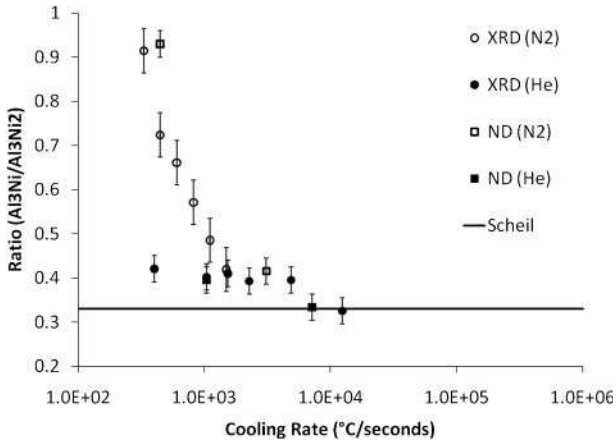

9 Neutron diffraction and XRD results for ratio of Al_3Ni to Al_3Ni_2 as function of cooling rate for two sets of Al–50 wt-%Ni samples: one was cooled in helium and the other in nitrogen

$$\lambda = 75{\cdot}38\dot{T}^{-0{\cdot}33} \quad (3)$$

$$\lambda = 69{\cdot}58\dot{T}^{-0{\cdot}33} \quad (4)$$

Particles of Al–36 wt-%Ni with diameters <180 μm were found to have a very different microstructure than those with larger sizes. The microstructure of such particle is shown in Fig. 7. The EDX analysis on the skeleton-like structure of this figure showed that it has a similar composition to Al_3Ni and no sign of any phase with composition close to Al_3Ni_2 was observed. Since the morphology of the Al_3Ni in Fig. 7 is not similar to those formed from the peritectic reaction, it is likely that in these particles, Al_3Ni has formed directly from the liquid. It is possible that the cooling rate in these particles was so high that the formation of Al_3Ni_2 and hence, the peritectic reaction was suppressed.

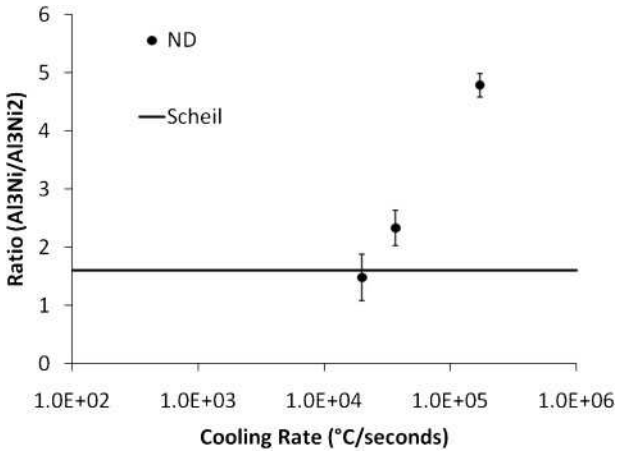

10 Neutron diffraction results for ratio of Al_3Ni to Al_3Ni_2 as function of cooling rate for Al–36 wt-%Ni cooled in helium

X-ray diffraction and ND

Phase fractions

Profile refinement was carried out using the software GSAS on both XRD and ND patterns from particles of Al–50 wt-%Ni and Al–36 wt-%Ni atomised in helium and in nitrogen. Figure 8 shows an example of measured ND pattern of Al–50 wt-%Ni with the diameter of 328 μm atomised in helium. Only three phases (i.e. Al_3Ni_2, Al_3Ni and Al) were identified in the entire size range that was investigated. Note that for the particles of Al–50 wt-%Ni, no trace of AlNi was found. A similar result has been reported in the literature for gas atomisation of Raney nickel alloy,[9] in spite of the fact that AlNi has been found to be the primary phase formed in a wide range of undercooling up to 320 K.[16] It is believed that AlNi transforms completely to Al_3Ni_2 during the peritectic reaction at 1133°C.

For each alloy, the ratio of Al_3Ni to Al_3Ni_2 was calculated from the Rietveld refinement to investigate the effect of cooling rate on the phase fractions after solidification. Figure 9 shows the ratio of Al_3Ni/Al_3Ni_2 as a function of cooling rate for Al–50 wt-%Ni atomised in helium (full symbols) and nitrogen (empty symbols). Note that the XRD data only come from the periphery of the particles, while the ND data are from the entire volume of the particles. Therefore, it can be assumed that, generally, the XRD data show the results of slightly higher cooling rates as the surface is expected to experience more rapid cooling. In addition, there is greater sampling error and more potential systematic errors associated with XRD.

It is evident in Fig. 9 that by increasing cooling rate, either by using helium rather than nitrogen, or by decreasing particle size, the ratio of Al_3Ni to Al_3Ni_2 approaches that of Scheil's prediction. This is the case in both XRD and ND results. After the formation of the first envelope of Al_3Ni around Al_3Ni_2, further transformation requires the diffusion of solute through

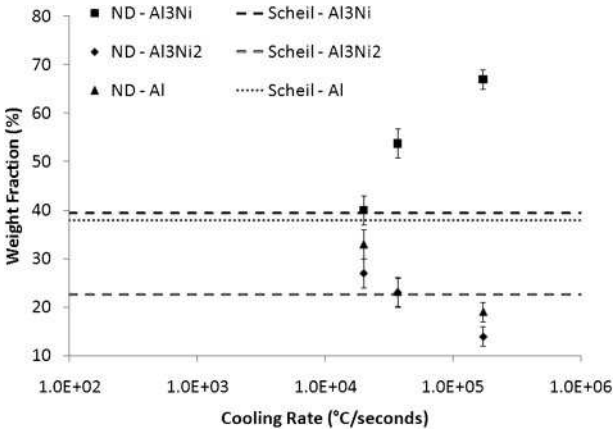

11 Weight fraction of Al_3Ni_2, Al_3Ni and Al as function of cooling rate of Al–36 wt%-Ni atomised in helium and Scheil–Gulliver's prediction for each phase

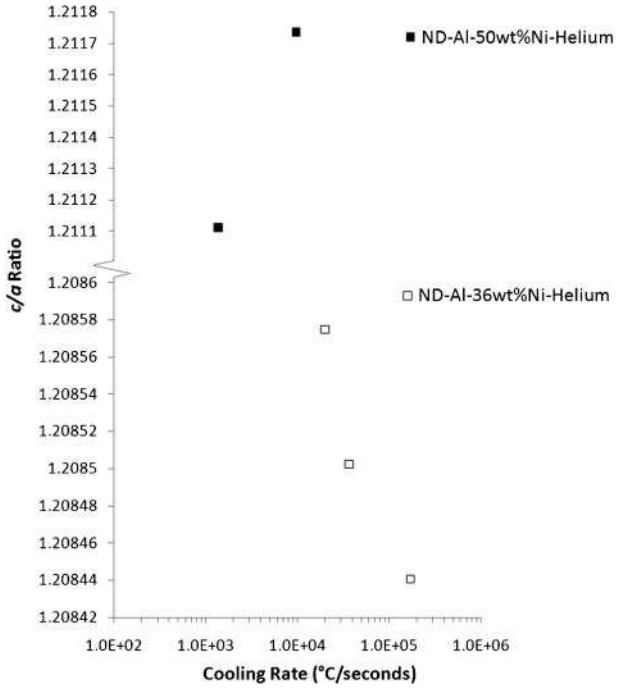

12 Lattice parameter ratio (*c*/*a*) of phase Al_3Ni_2 in Al–50 wt-%Ni (above) and Al–36 wt-%Ni (below)

that envelope. However, Al_3Ni has an exact stoichiometric composition. This eliminates the strong influence of having composition gradient through the envelope. Hence, the rate of transformation becomes extremely slow. It is likely that in a rapid solidification process, such a slow rate of transformation results in further suppression of the transformation. Since the Scheil–Gulliver equation does not account for peritectic transformation, it starts approaching the experimental values for the Al_3Ni fraction as the cooling rate increases.

The XRD results of particles of Al–36 wt-%Ni contained some unidentified peaks that made it difficult to perform Rietveld analysis. It is likely that the high cooling rate at the surface resulted in the formation of some metastable phases. Further investigation of these phases is underway. However, Rietveld refinement on ND patterns of particles of Al–36 wt-%Ni resulted in unexpected results. Figure 10 shows the ratio of Al_3Ni to Al_3Ni_2 as a function of cooling rate for the particles atomised in helium. It appears that the ratio decreases and approaches Scheil–Gulliver's prediction as the cooling rate decreases. Further investigation of the ND results shows that in the particles of Al–36 wt-%Ni, with decreasing cooling rate, the weight fraction of Al_3Ni decreases while the weight fraction of Al_3Ni_2 increases. It is likely that increasing cooling rate as a result of decreasing particle size results in the formation of Al_3Ni directly from the melt, as it is the case in particles <150 μm shown in Fig. 7. On the other hand, it is observed that the proportions of all three phases approach the Scheil–Gulliver prediction (Fig. 11).

Lattice parameter of Al_3Ni_2

By carrying out experiments approaching equilibrium conditions, Taylor and Doyle[8] showed that the *c*/*a* ratio for Al_3Ni_2 structure continuously decreases as the nickel content of Al_3Ni_2 decreases. They also suggested that the substitution of nickel atoms by aluminium atoms is responsible for the decrease in *c*/*a* ratio at the aluminium rich side of stoichiometric Al_3Ni_2.

Figure 12 illustrates the effect of cooling rate on the lattice parameter ratio (*c*/*a*) of Al_3Ni_2 in droplets of Al–36 wt-%Ni and Al–50 wt-%Ni. The data presented are for the results of refinement on ND patterns, since they better represent the average bulk value of lattice parameters in each sample. In addition, despite the fact that there are only two data points from ND experiment for Al–50 wt-%Ni and, hence, drawing a definite conclusion is not possible, they still show a very different trend from that of Al–36 wt-%Ni.

For Al–36 wt-%Ni, the Al_3Ni_2 is a metastable phase at room temperature. In addition, the *c*/*a* ratio for this phase is significantly $<1{\cdot}2132$, the stoichiometric *c*/*a* ratio of Al_3Ni_2, and it decreases with increasing cooling rate. On the other hand, for Al–50 wt-%Ni, the Al_3Ni_2 is a stable phase at room temperature. The *c*/*a* ratio in this alloy is much closer to the stoichiometric *c*/*a* ratio and it appears that it increases with increasing cooling rate.

From the phase diagram, it is obvious that the atomic percentage of nickel within the Al_3Ni_2 that forms from AlNi is significantly higher than that in the Al_3Ni_2 which forms directly from the liquid. This results in an increase in the *c*/*a* ratio as there are more nickel atoms in the lattice of Al_3Ni_2. In addition, it is possible that the observed differences are due to different formation mechanisms of Al_3Ni_2 in these alloys. In Al–36 wt-%Ni, the Al_3Ni_2 phase nucleates and grows directly from the liquid. In Al–50 wt-%Ni, it nucleates from the peritectic reaction of AlNi with the liquid and grows both from the peritectic transformation and from the liquid. With Al–36 wt-%Ni, by increasing cooling rate, it is possible that the number of trapped vacancies increases within the solid phase. This causes the relaxation of the lattice and hence, decreases the *c*/*a* ratio. However, with Al–50 wt-%Ni, during the transformation of AlNi to

Al_3Ni_2, increasing the cooling rate may not allow for the substitution of nickel atoms by aluminium atoms; therefore, the *c*/*a* ratio increases and it approaches the stoichiometric value of that in Al_3Ni_2. It is also shown that in Al–36 wt-%Ni, the weight fraction of Al_3Ni increases as the cooling rate increases while in Al–50 wt-% Ni, it decreases in the same conditions. If the changes of the fraction of Al_3Ni versus cooling rate in both alloys are compared with the trends of *c*/*a* ratio versus cooling rate in Fig. 12, it is observed that by increasing the weight fraction of Al_3Ni, the *c*/*a* ratio decreases in both alloys. In other words, it is likely that the atomic percentage of nickel in Al_3Ni_2 decreases as a result of the formation of Al_3Ni. Therefore, it is possible that besides different formation mechanisms, transformation of Al_3Ni_2 to Al_3Ni is also responsible for the reduction in *c*/*a* ratio. It is expected that some of the nickel atoms leave the Al_3Ni_2 phase to form Al_3Ni, which results in the reduction in lattice parameter.

Further experimental work and theoretical analysis are necessary to better understand the behaviour of *c*/*a* ratio in these alloys.

Conclusions

Powders of Al–50 wt-%Ni and Al–36 wt-%Ni were produced using the impulse atomisation technique. Microstructural analysis showed that finer microstructure was achieved in the smaller particle sizes and, also, when helium was used instead of nitrogen. Secondary dendrite arm spacing was used to estimate the solidification cooling rate. It was shown that particles of Al–36 wt-%Ni achieved higher cooling rate than those of Al–50 wt-%Ni. The XRD and ND were successfully used to estimate the phase fractions of the solidified powders. For each alloy, the ratio of Al_3Ni to Al_3Ni_2 was calculated from the Rietveld refinement to investigate the effect of cooling rate on the phase fractions after solidification. In addition, Scheil–Gulliver equation was applied to investigate the extent to which it can predict the phase fractions in these alloys. In Al–50 wt-%Ni, it was found that by increasing cooling rate, the ratio of Al_3Ni to Al_3Ni_2 approaches that of Scheil–Gulliver's prediction. This was attributed to the suppression of the peritectic transformation at high cooling rates. Opposite behaviour was observed in Al–36 wt-%Ni, where the ratio decreased and approached Scheil–Gulliver's prediction with decreasing cooling rate. This observation was related to the direct formation of Al_3Ni from the liquid and the suppression of Al_3Ni_2 formation. The effect of particle size and composition on the lattice parameter of Al_3Ni_2 was also discussed. In Al–36 wt-% Ni, the *c*/*a* ratio is significantly smaller than the stoichiometric *c*/*a* ratio of Al_3Ni_2, and it decreases with increasing cooling rate. On the other hand, for Al–50 wt-%Ni, the *c*/*a* ratio is much closer to the stoichiometric *c*/*a* ratio and it increases with increasing cooling rate. Different mechanisms of Al_3Ni_2 formation in the two alloys were discussed to explain the different behaviours of the *c*/*a* ratio.

Acknowledgements

This research was supported by Canadian Space Agency and by Natural Sciences and Engineering Research Council of Canada. This research at Oak Ridge National Laboratory's High Flux Isotope Reactor was sponsored by the Scientific User Facilities Division, Office of Basic Energy Sciences, US Department of Energy. In addition, the authors would like to thank National Research Council of Canada – Canadian Neutron Beam Centre, Chalk River, ON, Canada for their support in conducting the ND experiments. They are also thankful to Ulf Dahlborg, Monique Calvo-Dahlborg for their assistance in data analysis.

References

1. D. Tourret and Ch.-A. Gandin: 'A generalized segregation model for concurrent dendritic, peritectic and eutectic solidification', *Acta Mater.*, 2009, **57**, 2066–2079.
2. R. Siquieri, E. Doernberg, H. Emmerich and R. Schmid-Fetzer: 'Phase-field simulation of peritectic solidification closely coupled with directional solidification experiments in an Al–36 wt% Ni alloy', *J. Phys.: Condens. Matter*, 2009, **21**, 464112.
3. P. Nash, M. F. Singleton and J. L. Murray: 'Phase diagrams of binary nickel alloys'; 1991, Materials Park, OH, ASM.
4. D. H. St John and L. M. Hogan: 'A simple prediction of the rate of the peritectic transformation', *Acta Metall.*, 1987, **35**, (1), 171–174.
5. S. L. Chen, Y. Yang, S. W. Chen, X. G. Lu and Y. A. Chang: 'Solidification simulation using Scheil model in multicomponent systems', *J. Phase Equilib. Diffr.*, 2009, **30**, (5), 429–434.
6. A. Ilbagi, H. Henein and A. B. Phillion: 'Phase quantification of impulse atomized $Al_{68{\cdot}5}Ni_{31{\cdot}5}$ alloy', *J. Mater. Sci*, DOI number: 10.1007/s10853-010-4972-8.
7. A. Thevand, S. Poize, J.-P. Crousier and R. Streiff: 'Aluminization of nickel-formation of intermetallic phases and Ni_2Al_3 coatings', *J. Mater. Sci.*, 1981, **16**, (9), 2467–2479.
8. A. Taylor and N. J. Doyle: 'Further studies on the nickel–aluminium system. I. β-NiAl and δ-Ni2Al3 phase fields', *J. Appl. Cryst.*, 1972, **5**, 201–209.
9. C. M. Bao, U. Dahlborga, N. Adkins and M. Calvo-Dahlborg: 'Structural characterization of Al–Ni powders produced by gas atomisation', *J. Alloys Compd*, 2009, **481**, 199–206.
10. H. Henein: 'Single fluid atomization through the application of impulses to a melt', *Mater. Sci. Eng. A*, 2002, **A326**, (1), 92–100.
11. 'Standard test methods for metal powders and powder metallurgy products', Metal Powder Industries Federation, Princeton, NJ, USA, 1993.
12. A. C. Larson and R. B. von Dreele: 'General structure analysis system (GSAS)', Report LAUR 86-748, Los Alamos National Laboratory, Los Alamos, NM, USA, 2004.
13. B. H. Toby: 'EXPGUI, a graphical user interface for GSAS', *J. Appl. Cryst.*, 2001, **34**, 210–221.
14. W. M. Rohsenow, J. P. Hartnett and Y. I. Cho: 'Handbook of heat transfer', 3rd edn; 1998, New York, McGraw-Hill.
15. W. Kurz and D. J. Fisher: 'Fundamentals of solidification', 88; 1989, Aedermannsdorf, Transaction Technical Publication.
16. O. Shuleshova, D. Holland-Moritz, W. Loser, G. Reinhart, G. N. Iles and B. Buchner: 'Metastable formation of decagonal quasi-crystals during solidification of undercooled Al–Ni melts: *in situ* observations by synchrotron radiation', *EPL*, 2009, **86**, 36002.